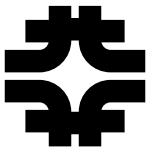

Fermi National Accelerator Laboratory

FERMILAB-Pub-97/076-E
CDF

Measurement of Diffractive Dijet Production at the Tevatron

F. Abe et al.
The CDF Collaboration

Fermi National Accelerator Laboratory
P.O. Box 500, Batavia, Illinois 60510

March 1997

Submitted to *Physical Review Letters*

Operated by Universities Research Association Inc. under Contract No. DE-AC02-76CH03000 with the United States Department of Energy

Disclaimer

Distribution

Measurement of Diffractive Dijet Production at the Tevatron

F. Abe,[16] H. Akimoto,[35] A. Akopian,[30] M. G. Albrow,[7] S. R. Amendolia,[26] D. Amidei,[19] J. Antos,[32] S. Aota,[35] G. Apollinari,[30] T. Asakawa,[35] W. Ashmanskas,[17] M. Atac,[7] F. Azfar,[25] P. Azzi-Bacchetta,[24] N. Bacchetta,[24] W. Badgett,[19] S. Bagdasarov,[30] M. W. Bailey,[21] J. Bao,[38] P. de Barbaro,[29] A. Barbaro-Galtieri,[17] V. E. Barnes,[28] B. A. Barnett,[15] M. Barone,[26] E. Barzi,[9] G. Bauer,[18] T. Baumann,[11] F. Bedeschi,[26] S. Behrends,[3] S. Belforte,[26] G. Bellettini,[26] J. Bellinger,[37] D. Benjamin,[34] J. Benlloch,[18] J. Bensinger,[3] D. Benton,[25] A. Beretvas,[7] J. P. Berge,[7] J. Berryhill,[5] S. Bertolucci,[9] B. Bevensee,[25] A. Bhatti,[30] K. Biery,[7] M. Binkley,[7] D. Bisello,[24] R. E. Blair,[1] C. Blocker,[3] A. Bodek,[29] W. Bokhari,[18] V. Bolognesi,[2] G. Bolla,[24] D. Bortoletto,[28] J. Boudreau,[27] L. Breccia,[2] C. Bromberg,[20] N. Bruner,[21] E. Buckley-Geer,[7] H. S. Budd,[29] K. Burkett,[19] G. Busetto,[24] A. Byon-Wagner,[7] K. L. Byrum,[1] J. Cammerata,[15] C. Campagnari,[7] M. Campbell,[19] A. Caner,[26] W. Carithers,[17] D. Carlsmith,[37] A. Castro,[24] D. Cauz,[26] Y. Cen,[29] F. Cervelli,[26] P. S. Chang,[32] P. T. Chang,[32] H. Y. Chao,[32] J. Chapman,[19] M. -T. Cheng,[32] G. Chiarelli,[26] T. Chikamatsu,[35] C. N. Chiou,[32] L. Christofek,[13] S. Cihangir,[7] A. G. Clark,[10] M. Cobal,[26] E. Cocca,[26] M. Contreras,[5] J. Conway,[31] J. Cooper,[7] M. Cordelli,[9] C. Couyoumtzelis,[10] D. Crane,[1] D. Cronin-Hennessy,[6] R. Culbertson,[5] T. Daniels,[18] F. DeJongh,[7] S. Delchamps,[7] S. Dell'Agnello,[26] M. Dell'Orso,[26] R. Demina,[7] L. Demortier,[30] M. Deninno,[2] P. F. Derwent,[7] T. Devlin,[31] J. R. Dittmann,[6] S. Donati,[26] J. Done,[33] T. Dorigo,[24] A. Dunn,[19] N. Eddy,[19] K. Einsweiler,[17] J. E. Elias,[7] R. Ely,[17] E. Engels, Jr.,[27] D. Errede,[13] S. Errede,[13] Q. Fan,[29] G. Feild,[38] C. Ferretti,[26] I. Fiori,[2] B. Flaugher,[7] G. W. Foster,[7] M. Franklin,[11] M. Frautschi,[34] J. Freeman,[7] J. Friedman,[18] H. Frisch,[5] Y. Fukui,[16] S. Funaki,[35] S. Galeotti,[26] M. Gallinaro,[24] O. Ganel,[34] M. Garcia-Sciveres,[17] A. F. Garfinkel,[28] C. Gay,[11] S. Geer,[7] D. W. Gerdes,[15] P. Giannetti,[26] N. Giokaris,[30] P. Giromini,[9] G. Giusti,[26] L. Gladney,[25] D. Glenzinski,[15] M. Gold,[21] J. Gonzalez,[25] A. Gordon,[11] A. T. Goshaw,[6] Y. Gotra,[24] K. Goulianos,[30] H. Grassmann,[26] L. Groer,[31] C. Grosso-Pilcher,[5] G. Guillian,[19] R. S. Guo,[32] C. Haber,[17] E. Hafen,[18]

S. R. Hahn,[7] R. Hamilton,[11] R. Handler,[37] R. M. Hans,[38] F. Happacher,[26] K. Hara,[35] A. D. Hardman,[28] B. Harral,[25] R. M. Harris,[7] S. A. Hauger,[6] J. Hauser,[4] C. Hawk,[31] E. Hayashi,[35] J. Heinrich,[25] K. D. Hoffman,[28] M. Hohlmann,[5] C. Holck,[25] R. Hollebeek,[25] L. Holloway,[13] A. Hölscher,[14] S. Hong,[19] G. Houk,[25] P. Hu,[27] B. T. Huffman,[27] R. Hughes,[22] J. Huston,[20] J. Huth,[11] J. Hylen,[7] H. Ikeda,[35] M. Incagli,[26] J. Incandela,[7] G. Introzzi,[26] J. Iwai,[35] Y. Iwata,[12] H. Jensen,[7] U. Joshi,[7] R. W. Kadel,[17] E. Kajfasz,[24] H. Kambara,[10] T. Kamon,[33] T. Kaneko,[35] K. Karr,[36] H. Kasha,[38] Y. Kato,[23] T. A. Keaffaber,[28] L. Keeble,[9] K. Kelley,[18] R. D. Kennedy,[7] R. Kephart,[7] P. Kesten,[17] D. Kestenbaum,[11] R. M. Keup,[13] H. Keutelian,[7] F. Keyvan,[4] B. Kharadia,[13] B. J. Kim,[29] D. H. Kim,[7a] H. S. Kim,[14] S. B. Kim,[19] S. H. Kim,[35] Y. K. Kim,[17] L. Kirsch,[3] P. Koehn,[29] K. Kondo,[35] J. Konigsberg,[8] S. Kopp,[5] K. Kordas,[14] A. Korytov,[8] W. Koska,[7] E. Kovacs,[7a] W. Kowald,[6] M. Krasberg,[19] J. Kroll,[7] M. Kruse,[29] T. Kuwabara,[35] S. E. Kuhlmann,[1] E. Kuns,[31] A. T. Laasanen,[28] S. Lammel,[7] J. I. Lamoureux,[3] T. LeCompte,[1] S. Leone,[26] J. D. Lewis,[7] P. Limon,[7] M. Lindgren,[4] T. M. Liss,[13] N. Lockyer,[25] O. Long,[25] C. Loomis,[31] M. Loreti,[24] J. Lu,[33] D. Lucchesi,[26] P. Lukens,[7] S. Lusin,[37] J. Lys,[17] K. Maeshima,[7] A. Maghakian,[30] P. Maksimovic,[18] M. Mangano,[26] J. Mansour,[20] M. Mariotti,[24] J. P. Marriner,[7] A. Martin,[38] J. A. J. Matthews,[21] R. Mattingly,[18] P. McIntyre,[33] P. Melese,[30] A. Menzione,[26] E. Meschi,[26] S. Metzler,[25] C. Miao,[19] T. Miao,[7] G. Michail,[11] R. Miller,[20] H. Minato,[35] S. Miscetti,[9] M. Mishina,[16] H. Mitsushio,[35] T. Miyamoto,[35] S. Miyashita,[35] N. Moggi,[26] Y. Morita,[16] J. Mueller,[27] A. Mukherjee,[7] T. Muller,[4] P. Murat,[26] H. Nakada,[35] I. Nakano,[35] C. Nelson,[7] D. Neuberger,[4] C. Newman-Holmes,[7] C.-Y. Ngan,[18] M. Ninomiya,[35] L. Nodulman,[1] S. H. Oh,[6] K. E. Ohl,[38] T. Ohmoto,[12] T. Ohsugi,[12] R. Oishi,[35] M. Okabe,[35] T. Okusawa,[23] R. Oliveira,[25] J. Olsen,[37] C. Pagliarone,[2] R. Paoletti,[26] V. Papadimitriou,[34] S. P. Pappas,[38] N. Parashar,[26] S. Park,[7] A. Parri,[9] J. Patrick,[7] G. Pauletta,[26] M. Paulini,[17] A. Perazzo,[26] L. Pescara,[24] M. D. Peters,[17] T. J. Phillips,[6] G. Piacentino,[2] M. Pillai,[29] K. T. Pitts,[7] R. Plunkett,[7] L. Pondrom,[37] J. Proudfoot,[1] F. Ptohos,[11] G. Punzi,[26] K. Ragan,[14] D. Reher,[17] A. Ribon,[24] F. Rimondi,[2] L. Ristori,[26] W. J. Robertson,[6] T. Rodrigo,[26] S. Rolli,[26] J. Romano,[5] L. Rosenson,[18] R. Roser,[13] W. K. Sakumoto,[29] D. Saltzberg,[5] A. Sansoni,[9]

L. Santi,[26] H. Sato,[35] P. Schlabach,[7] E. E. Schmidt,[7] M. P. Schmidt,[38] A. Scribano,[26] S. Segler,[7] S. Seidel,[21] Y. Seiya,[35] G. Sganos,[14] M. D. Shapiro,[17] N. M. Shaw,[28] Q. Shen,[28] P. F. Shepard,[27] M. Shimojima,[35] M. Shochet,[5] J. Siegrist,[17] A. Sill,[34] P. Sinervo,[14] P. Singh,[27] J. Skarha,[15] K. Sliwa,[36] F. D. Snider,[15] T. Song,[19] J. Spalding,[7] T. Speer,[10] P. Sphicas,[18] F. Spinella,[26] M. Spiropulu,[11] L. Spiegel,[7] L. Stanco,[24] J. Steele,[37] A. Stefanini,[26] K. Strahl,[14] J. Strait,[7] R. Ströhmer,[7a] D. Stuart,[7] G. Sullivan,[5] A. Soumarokov,[32] K. Sumorok,[18] J. Suzuki,[35] T. Takada,[35] T. Takahashi,[23] T. Takano,[35] K. Takikawa,[35] N. Tamura,[12] B. Tannenbaum,[21] F. Tartarelli,[26] W. Taylor,[14] P. K. Teng,[32] Y. Teramoto,[23] S. Tether,[18] D. Theriot,[7] T. L. Thomas,[21] R. Thun,[19] M. Timko,[36] P. Tipton,[29] A. Titov,[30] S. Tkaczyk,[7] D. Toback,[5] K. Tollefson,[29] A. Tollestrup,[7] W. Trischuk,[14] J. F. de Troconiz,[11] S. Truitt,[19] J. Tseng,[18] N. Turini,[26] T. Uchida,[35] N. Uemura,[35] F. Ukegawa,[25] G. Unal,[25] J. Valls,[7a] S. C. van den Brink,[27] S. Vejcik, III,[19] G. Velev,[26] R. Vidal,[7] M. Vondracek,[13] D. Vucinic,[18] R. G. Wagner,[1] R. L. Wagner,[7] J. Wahl,[5] N. B. Wallace,[26] A. M. Walsh,[31] C. Wang,[6] C. H. Wang,[32] J. Wang,[5] M. J. Wang,[32] Q. F. Wang,[30] A. Warburton,[14] T. Watts,[31] R. Webb,[33] C. Wei,[6] C. Wendt,[37] H. Wenzel,[17] W. C. Wester, III,[7] A. B. Wicklund,[1] E. Wicklund,[7] R. Wilkinson,[25] H. H. Williams,[25] P. Wilson,[5] B. L. Winer,[22] D. Winn,[19] D. Wolinski,[19] J. Wolinski,[20] S. Worm,[21] X. Wu,[10] J. Wyss,[24] A. Yagil,[7] W. Yao,[17] K. Yasuoka,[35] Y. Ye,[14] G. P. Yeh,[7] P. Yeh,[32] M. Yin,[6] J. Yoh,[7] C. Yosef,[20] T. Yoshida,[23] D. Yovanovitch,[7] I. Yu,[7] L. Yu,[21] J. C. Yun,[7] A. Zanetti,[26] F. Zetti,[26] L. Zhang,[37] W. Zhang,[25] and S. Zucchelli[2]

(CDF Collaboration)

[1] *Argonne National Laboratory, Argonne, Illinois 60439*

[2] *Istituto Nazionale di Fisica Nucleare, University of Bologna, I-40127 Bologna, Italy*

[3] *Brandeis University, Waltham, Massachusetts 02264*

[4] *University of California at Los Angeles, Los Angeles, California 90024*

[5] *University of Chicago, Chicago, Illinois 60638*

[6] *Duke University, Durham, North Carolina 28708*

[7] *Fermi National Accelerator Laboratory, Batavia, Illinois 60510*

[8] *University of Florida, Gainesville, FL 33611*

[9] *Laboratori Nazionali di Frascati, Istituto Nazionale di Fisica Nucleare, I-00044 Frascati, Italy*

[10] *University of Geneva, CH-1211 Geneva 4, Switzerland*

[11] *Harvard University, Cambridge, Massachusetts 02138*

[12] *Hiroshima University, Higashi-Hiroshima 724, Japan*

[13] *University of Illinois, Urbana, Illinois 61801*

[14] *Institute of Particle Physics, McGill University, Montreal H3A 2T8, and University of Toronto, Toronto M5S 1A7, Canada*

[15] *The Johns Hopkins University, Baltimore, Maryland 21218*

[16] *National Laboratory for High Energy Physics (KEK), Tsukuba, Ibaraki 315, Japan*

[17] *Ernest Orlando Lawrence Berkeley National Laboratory, Berkeley, California 94720*

[18] *Massachusetts Institute of Technology, Cambridge, Massachusetts 02139*

[19] *University of Michigan, Ann Arbor, Michigan 48109*

[20] *Michigan State University, East Lansing, Michigan 48824*

[21] *University of New Mexico, Albuquerque, New Mexico 87132*

[22] *The Ohio State University, Columbus, OH 43320*

[23] *Osaka City University, Osaka 588, Japan*

[24] *Universita di Padova, Istituto Nazionale di Fisica Nucleare, Sezione di Padova, I-36132 Padova, Italy*

[25] *University of Pennsylvania, Philadelphia, Pennsylvania 19104*

[26] *Istituto Nazionale di Fisica Nucleare, University and Scuola Normale Superiore of Pisa, I-56100 Pisa, Italy*

[27] *University of Pittsburgh, Pittsburgh, Pennsylvania 15270*

[28] *Purdue University, West Lafayette, Indiana 47907*

[29] *University of Rochester, Rochester, New York 14628*

[30] *Rockefeller University, New York, New York 10021*

[31] *Rutgers University, Piscataway, New Jersey 08854*

[32] *Academia Sinica, Taipei, Taiwan 11530, Republic of China*

[33] *Texas A&M University, College Station, Texas 77843*

[34] *Texas Tech University, Lubbock, Texas 79409*

[35] *University of Tsukuba, Tsukuba, Ibaraki 315, Japan*

[36] *Tufts University, Medford, Massachusetts 02155*

[37] *University of Wisconsin, Madison, Wisconsin 53806*

[38] *Yale University, New Haven, Connecticut 06511*

Abstract

We report the observation and measurement of the rate of diffractive dijet production at the Fermilab Tevatron $\bar{p}p$ collider at $\sqrt{s}$=1.8 TeV. In events with two jets of $E_T > 20$ GeV, $1.8 < |\eta| < 3.5$ and $\eta_1 \eta_2 > 0$, we find that the diffractive to non-diffractive production ratio is $R_{JJ} = [0.75 \pm 0.05(stat) \pm 0.09(syst)]\%$. By comparing this result, in combination with our measured rate for diffractive W boson production reported previously, with predictions based on a hard partonic pomeron structure, we determine the pomeron gluon fraction to be $f_g = 0.7 \pm 0.2$.

PACS number(s): 13.87.Ce, 12.38.Qk, 12.40.Nn

As part of a program to probe the partonic structure of the pomeron [1] at the Collider Detector at Fermilab (CDF), we have measured the rate of production of two-jet (dijet) events in $p\bar{p}$ single diffraction dissociation, $p+\bar{p} \to p(\bar{p})+X(\to Jet1+Jet2+X')$, at $\sqrt{s} = 1.8$ TeV. Diffractive events are identified by the characteristic signature of a large rapidity [2] gap (region of rapidity devoid of particles) between the outgoing recoil $p(\bar{p})$ and the particles in X. The recoil nucleon escapes at high rapidity retaining a large fraction x (typically $x > 0.95$) of its initial longitudinal momentum. The rapidity gap arises from the colorless nature of the pomeron ($\mathcal{P}$), which is presumed to be exchanged in diffractive processes [1,3]. It has been proposed [4] that the production rate and kinematics of diffractively produced dijet events can be used to probe the partonic structure of the pomeron.

Diffractive dijets were first observed by the UA8 experiment at CERN in $p\bar{p}$ collisions at $\sqrt{s} = 630$ GeV [5]. The topology of the UA8 events is consistent with a dominant hard partonic pomeron structure of the form $\beta G(\beta) \sim \beta(1-\beta)$, where β is the momentum fraction of the parton in the pomeron. However, the event topology alone cannot distinguish between a hard-quark or a hard-gluon structure, while the dijet production rate, which is sensitive to the quark/gluon ratio, is model dependent. The quark/gluon ratio may be determined in a model-independent way by performing two experiments with different sensitivity to the quark and gluon pomeron content. This was done by the ZEUS collaboration at HERA by measuring diffractive deep inelastic scattering, which probes quarks directly, and diffractive jet photoproduction, which probes both quarks and gluons. From these measurements, ZEUS determined [6] that the gluon fraction of the hard partonic component of the pomeron, f_g, is in the range $0.3 < f_g < 0.8$. This fraction can also be determined in $p\bar{p}$ collisions at the Tevatron from the rate of diffractive W production, which is sensitive to the quark component, and that of dijets, which is sensitive to both the quark and gluon components of the pomeron. In a previous paper [7] we reported the results of a measurement of diffractive W production. Here, we report results on diffractive dijet production and combine them with our W results to extract the quark/gluon ratio of the pomeron structure.

The present measurement is based on 2.2 pb^{-1} of data collected during 1994-95 using

a trigger requiring two high transverse energy (E_T) forward jets. In our analysis, the two most energetic (leading) jets in an event were required to have transverse energy $E_T > 20$ GeV within an $\eta - \phi$ cone of radius 0.7 around the jet axis, pseudorapidity $1.8 < |\eta| < 3.5$ and $\eta_1 \eta_2 > 0$. No requirement was imposed on additional jets in an event. Because of the high instantaneous luminosity during data collection, about 73% of the dijet events have superimposed one or more "minimum bias" events produced by additional interactions occurring in the same beam crossing. Since the overlay of extra events would most likely obscure a diffractive rapidity gap, events with two or more reconstructed vertices were removed from the data sample, leaving 30352 single vertex events.

The CDF detector is described in detail elsewhere [8]. In the rapidity gap analysis we use the "Beam-Beam Counters" (BBC) and the calorimeters. The BBC consist of a square array of eight vertical and eight horizontal scintillation counters perpendicular to the beam line, placed at a z-position of 6 m from the center of the detector and covering approximately the region $3.2 < |\eta| < 5.9$. The calorimeters have projective tower geometry and cover the regions $|\eta| < 1.1$ (central), $1.1 < |\eta| < 2.4$ (plug), and $2.2 < |\eta| < 4.2$ (forward). The $\Delta\eta \times \Delta\phi$ tower size is $0.1 \times 15^\circ$ in the central and $0.1 \times 5^\circ$ in the plug and forward calorimeters.

Figure 1 shows the distributions of $E_T^{(1)}$ and η_1 of the leading jet, and of $\Delta E_T = E_T^{(1)} - E_T^{(2)}$ and $\Delta\phi = \phi_1 - \phi_2$ of the two leading jets for the single vertex event sample. The two leading jets tend to be balanced both in E_T and ϕ. The E_T and η distributions of the third most energetic jet with $E_T^{(3)} > 5$ GeV are also shown. Our analysis is based on counting BBC multiplicity (hits), within $3.2 < |\eta| < 5.9$, and calorimeter towers with energy above 1.5 GeV, within $2.4 < |\eta| < 4.2$, in the η-region opposite the dijet side. The tower energy threshold of 1.5 GeV is used to suppress calorimeter noise. Figure 2 shows the BBC multiplicity, N_{BBC}, versus forward calorimeter tower multiplicity opposite in η to the dijet system, N_T, for all single vertex events. The distinct peak in the "0-0" bin, $N_{BBC} = N_T = 0$, is attributed to diffractive dijet events with a forward rapidity gap. The number of diffractively produced events in the total event sample is determined from the number of events above background

in this peak, taking into account the single vertex cut efficiency, the livetime acceptance of the BBC and forward calorimeter triggers, and the acceptance for diffractive events with a rapidity gap, as explained below.

The single vertex cut efficiency was determined from a study of the number of single vertex events as a function of instantaneous luminosity. This study showed that the single vertex requirement we used, in addition to rejecting events with multiple interactions, rejected a substantial fraction of single interaction dijet events because of multiple reconstructed vertices. The efficiency in retaining single interaction dijet events was measured to be $0.58 \pm 0.05(syst)$ for no-gap (NG) events, namely events with no rapidity gap in the region $|\eta| > 2.4$ of our measurement. For rapidity gap (RG) events, the single vertex efficiency was determined to be 0.86 ± 0.03 by comparing the number of RG events in the single vertex sample with the number found in the entire sample of events. Thus, the ratio of RG to NG events found in the single vertex sample must be multiplied by the single vertex efficiency ratio of $(0.58 \pm 0.05)/(0.86 \pm 0.03) = 0.67 \pm 0.06$ to take into account the single vertex relative efficiency between gap and no-gap events.

The BBC and calorimeter livetime acceptance was measured using a sample of 98000 events collected with the detector triggered on beam crossings only. It was found that a fraction of 0.15 ± 0.02 of the events with no vertex in this sample have one or more calorimeter towers with energy above 1.5 GeV and/or one or more BBC counts. This occupancy level, which includes calorimeter noise as well as any beam-associated calorimeter energy or BBC hits, corresponds to a livetime acceptance of 0.85 ± 0.02, which is used to correct the data for the resulting 15% loss of RG events.

The expected RG acceptance is calculated using the POMPYT [9] and PYTHIA [10] Monte Carlo (MC) programs. All our MC simulations are followed by a simulation of the CDF detector. POMPYT is based on the Ingelman-Schlein model [4], in which a flux of pomerons carried by the $p(\bar{p})$ interacts with the $\bar{p}(p)$ in a manner prescribed by PYTHIA. We use a hard pomeron structure function of the form $\beta G(\beta) = 6\beta(1-\beta)$ and the *standard* [11] pomeron flux factor, $f_{p/p}(\xi, t) = K\xi^{1-2\alpha(t)}\ F^2(t)$, where ξ is the fraction of the beam

momentum carried by the pomeron, $\alpha(t) = 1.115 + 0.26\,t$ is the pomeron Regge trajectory, $F(t)$ the proton form factor, and $K = 0.73$ GeV^{-2}. For the numerical values of the parameters used see Ref. [11]. Under these assumptions, we obtain for the 0-0 bin of Fig. 2 a diffractive gap-acceptance of 0.70 ± 0.03. The non-diffractive background under the diffractive peak is evaluated by a smooth two dimensional extrapolation from the adjacent BBC and calorimeter bins, taking into account the diffractive acceptance of these bins. There are $202 \pm 14(stat) \pm 10(syst)$ events above background. The ratio, R_{JJ}, of all diffractive to non-diffractive dijet events is obtained by dividing this number by the livetime and gap acceptances and by the total number of the NG single vertex events, and multiplying by the single vertex relative efficiency. The final result is

$$R_{JJ} = [0.75 \pm 0.05(stat) \pm 0.09(syst)]\%$$

We now compare some characteristics of the events in the 0-0 bin of Fig. 2, which we refer to as "diffractive" although they contain an estimated 20% non-diffractive background, to those of non-diffractive events (outside the 0-0 bin). Figures 3a and 3b show the average η and average E_T distributions, respectively, of the two leading jets for diffractive (solid) and non-diffractive (dashed) events. The corresponding distributions are very similar. The difference $\Delta\phi = \phi_1 - \phi_2$ between the azimuthal angles of the two leading jets in an event, shown in Fig. 3c, appears to be more peaked for diffractive than for non-diffractive events. About 45% of the diffractive events have a third jet of $E_T^{(3)} > 5$ GeV, as compared to 73% of the non-diffractive sample. The diffractive events have a softer $E_T^{(3)}$ distribution (Fig. 3d), as expected from their sharper $\Delta\phi$ distribution (Fig. 3c). Figure 4 shows the MC generated pomeron ξ distribution for diffractive dijets with jet $E_T > 20$ GeV and $1.8 < |\eta| < 3.5$. The shaded area represents events with a BBC and forward calorimeter rapidity gap as used in this analysis. The events are concentrated at $0.005 < \xi < 0.015$.

The ratio of diffractive to non-diffractive dijets calculated with POMPYT using the standard pomeron flux and a hard-gluon (quark) pomeron structure of the form $\beta G(\beta) \sim \beta(1-\beta)$ is 5% (2%). Assuming that only hard partons carrying a fraction D of the total

pomeron momentum participate in dijet production, D can be evaluated as a function of the gluon fraction, f_g, of the hard component of the pomeron by comparing the experimental value of R_{JJ} with the MC predictions. Figure 5 shows curves for D versus f_g corresponding to the $\pm 1\,\sigma$ values of R_{JJ}. Also shown are curves obtained from our measured diffractive W fraction [7], $R_W = (1.15 \pm 0.55)\%$, and the corresponding standard flux predictions. The $\pm 1\,\sigma$ limits from the W measurement are shown as dotted (solid) lines for two (three) quark flavors in the pomeron (u,d or u,d,s). The dashed lines show the UA8 result [12] and the dashed-dotted lines the ZEUS result [6]. The UA8 result is in agreement with our more precise measurement. From the diamond-shaped region in Fig. 5, enclosed by our dijet curves on top and bottom and our W curves for two (three) quark flavors on the left (right), we determine the gluon fraction to be $f_g = 0.7 \pm 0.2$ and the momentum fraction $D = 0.18 \pm 0.04$. The gluon fraction, which does not depend on the pomeron flux normalization or on the validity of the momentum sum rule for the pomeron, agrees with the ZEUS result of $0.3 < f_g < 0.8$. However, the momentum fraction we measure is well below the range of $0.4 < D < 1.6$ reported by ZEUS. The difference in the D factors cannot be explained by the Q^2 evolution of the pomeron structure function. From the Q^2 dependece of the quark and gluon fractions obtained by the H1 Collaboration from a QCD analysis of diffractive DIS data collected at HERA [13], we estimate the effect of the Q^2 evolution on D to be of $\mathcal{O}(10\%)$. The observed discrepancy implies a breakdown of factorization as used in Ref. [4] and in POMPYT. Since the diffractive rates depend on the product of the factor D times the pomeron flux (luminosity), the apparent decrease of D at the Tevatron could be due to a decrease in the pomeron flux.

The hard-quark content in the pomeron structure may be the reason for the observed reduced third jet activity and the narrower $\Delta\phi$ distribution in diffractive events (Figs. 3c,d). Monte Carlo simulations, using POMPYT with a full gluon (quark) pomeron structure to simulate diffractive and PYTHIA to simulate non-diffractive events, predict a value of 0.89 (0.38) for the ratio of diffractive to non-diffractive fractions of events with a third jet of $E_T^{(3)} > 5$ GeV. Using our measured gluon fraction, the predicted ratio is 0.73 ± 0.11. This

value is consistent with the ratio of $0.62 \pm 0.05(stat)$ derived by dividing the measured fractions of 45% and 73% of events with a third jet of $E_T^{(3)} > 5$ GeV in the diffractive and non-diffractive event samples, respectively.

In conclusion, in a sample of events with two jets of $E_T > 20$ GeV, $1.8 < |\eta| < 3.5$ and $\eta_1 \eta_2 > 0$, we have measured the ratio of diffractive to non-diffractive dijet production to be $R_{JJ} = [0.75 \pm 0.05(stat) \pm 0.09(syst)]\%$. Assuming a hard gluon and quark pomeron structure of the form $\beta G(\beta) \sim \beta(1-\beta)$, and by comparing this result with our diffractive W production rate and Monte Carlo predictions, we determine the hard-gluon pomeron content to be $f_g = 0.7 \pm 0.2$. This result is independent of the pomeron flux normalization or of the validity of the momentum sum rule for the pomeron. Based on dijet and W rate predictions using the standard pomeron flux, we further determine the fraction of the total pomeron momentum carried by its partons to be $D = 0.18 \pm 0.04$. If the momentum sum rule is assumed to hold, the deviation of the value of D from unity may be interpreted as a discrepancy on the pomeron flux normalization,, as suggested in Ref. [11].

We thank the Fermilab staff and the technical staffs of the participating institutions for their vital contributions. This work was supported by the U.S. Department of Energy and National Science Foundation; the Italian Istituto Nazionale di Fisica Nucleare; the Ministry of Education, Science and Culture of Japan; the Natural Sciences and Engineering Research Council of Canada; the National Science Council of the Republic of China; and the A. P. Sloan Foundation.

REFERENCES

[1] See P.D.B. Collins, An Introduction to Regge Theory and High Energy Physics, Cambridge University Press, Cambridge (1977).

[2] In this paper, we use rapidity pseudorapidity, η, interchangeably; $\eta \equiv -\ln(\tan\frac{\theta}{2})$, where θ is the polar angle of a particle with respect to the proton beam direction. The azimuthal angle is denoted by ϕ, and the transverse energy of a jet, E_T, is defined as $E\sin\theta$.

[3] K. Goulianos, Phys. Reports **101**, 169 (1983).

[4] G. Ingelman and P. Schlein, Phys. Lett. **B152**, 256 (1985).

[5] A. Brandt *et al.*, Phys. Lett. **B297**, 417 (1992).

[6] M. Derrick *et al.*, Phys. Lett. **B356**, 129 (1995).

[7] F. Abe *et al.*, CDF Collaboration, "Observation of Diffractive W-Boson Production at the Tevatron", submitted to Phys. Rev. Letters.

[8] F. Abe *et al.*, Nucl. Instrum. Methods **A271**, 387 (1988).

[9] P. Bruni and G. Ingelman, Preprint DESY-93-187; Proceedings of the International Europhysics Conference on High Energy Physics, Marseille, France, 22-28 July 1993, Editions Frontières (Eds. J. Carr and M. Perrottet).

[10] T. Sjöstrand, Comput. Phys. Commun. **82**, 74 (1994).

[11] K. Goulianos, Phys. Lett. **B358**, 379 (1995).

[12] P. Schlein, "Evidence for Partonic Behavior of the Pomeron", Proceedings of the International Europhysics Conference on High Energy Physics, Marseille, France, 22-28 July 1993, Editions Frontières (Eds. J. Carr and M. Perrottet).

[13] H1 Collaboration, "A Measurement and QCD Analysis of the Diffractive Structure Function $F_2^{D(3)}$", Submitted to the 28th International Conference on High Energy

Physics ICHEP'96, Warsaw, Poland, July 1996.

FIGURES

FIG. 1. (*top*) Leading jet transverse energy and pseudorapidity; (*middle*) difference between the transverse energies and azimuthal angles of the two leading jets; (*bottom*) third jet ($E_T^{(3)} > 5$ GeV) transverse energy and pseudorapidity (solid/dashed line for events with the two leading jets at positive/negative η).

FIG. 2. Beam-beam counter multiplicity (BBC hits) versus forward calorimeter tower multiplicity in the pseudorapidity regions $3.2 < |\eta_{(BBC)}| < 5.9$ and $2.4 < |\eta_{(TOWER)}| < 4.2$ opposite the dijet system.

FIG. 3. Comparison of diffractive (solid) with normalized non-diffractive (dashed) event distributions: (a) average pseudorapidity, (b) average transverse energy and (c) azimuthal angle difference of the two leading jets, and (d) transverse energy of the third jet. The diffractive event sample is from the 0-0 bin of Fig. 2, which contains approximately 20% non-diffractive background.

FIG. 4. Pomeron ξ distribution for diffractive dijet events with jet $E_T > 20$ GeV and $1.8 < |\eta| < 3.5$ generated by POMPYT using a hard-gluon pomeron structure. The shaded area represents the subset of Monte Carlo events with zero BBC and forward calorimeter multiplicities, corresponding to the data in the (0,0) bin of Fig. 2.

FIG. 5. Momentum fraction versus gluon fraction of hard partons in the pomeron evaluated by comparing measured diffractive rates with Monte Carlo predictions based on the standard pomeron flux and assuming that only hard pomeron partons participate in the diffractive processes considered. Results are shown for ZEUS (dashed-dotted), UA8 (dashed) and the CDF-DIJET and CDF-W measurements. The CDF W result is shown for two (dotted) or three (solid) light quark flavors in the pomeron . The shaded region is used in the text to extract the quark to gluon fraction of the pomeron and the standard flux discrepancy factor.

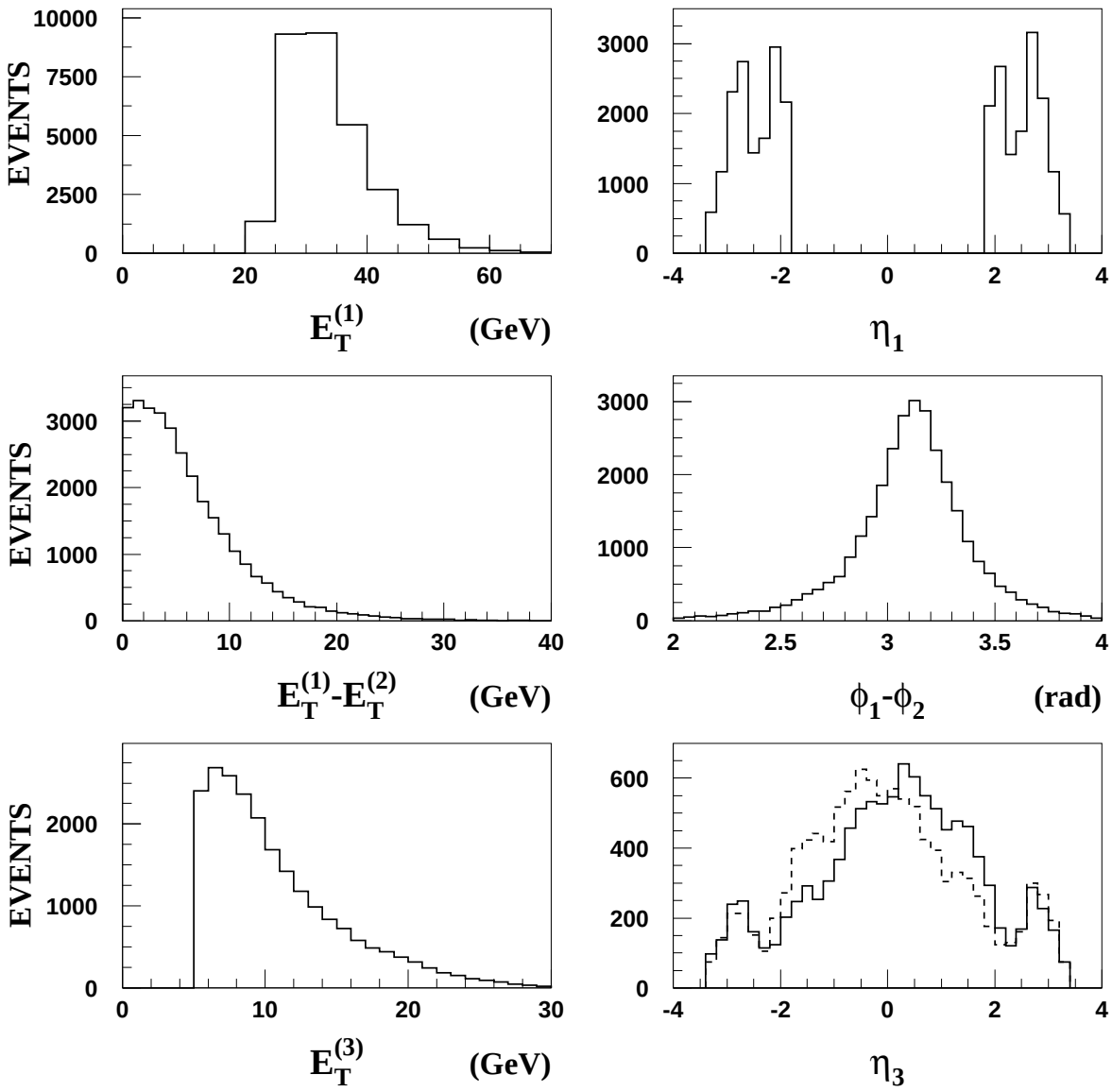

FIG. 1. (*top*) Leading jet transverse energy and pseudorapidity; (*middle*) difference between the transverse energies and azimuthal angles of the two leading jets; (*bottom*) third jet ($E_T^{(3)} > 5$ GeV) transverse energy and pseudorapidity (solid/dashed line for events with the two leading jets at positive/negative η).

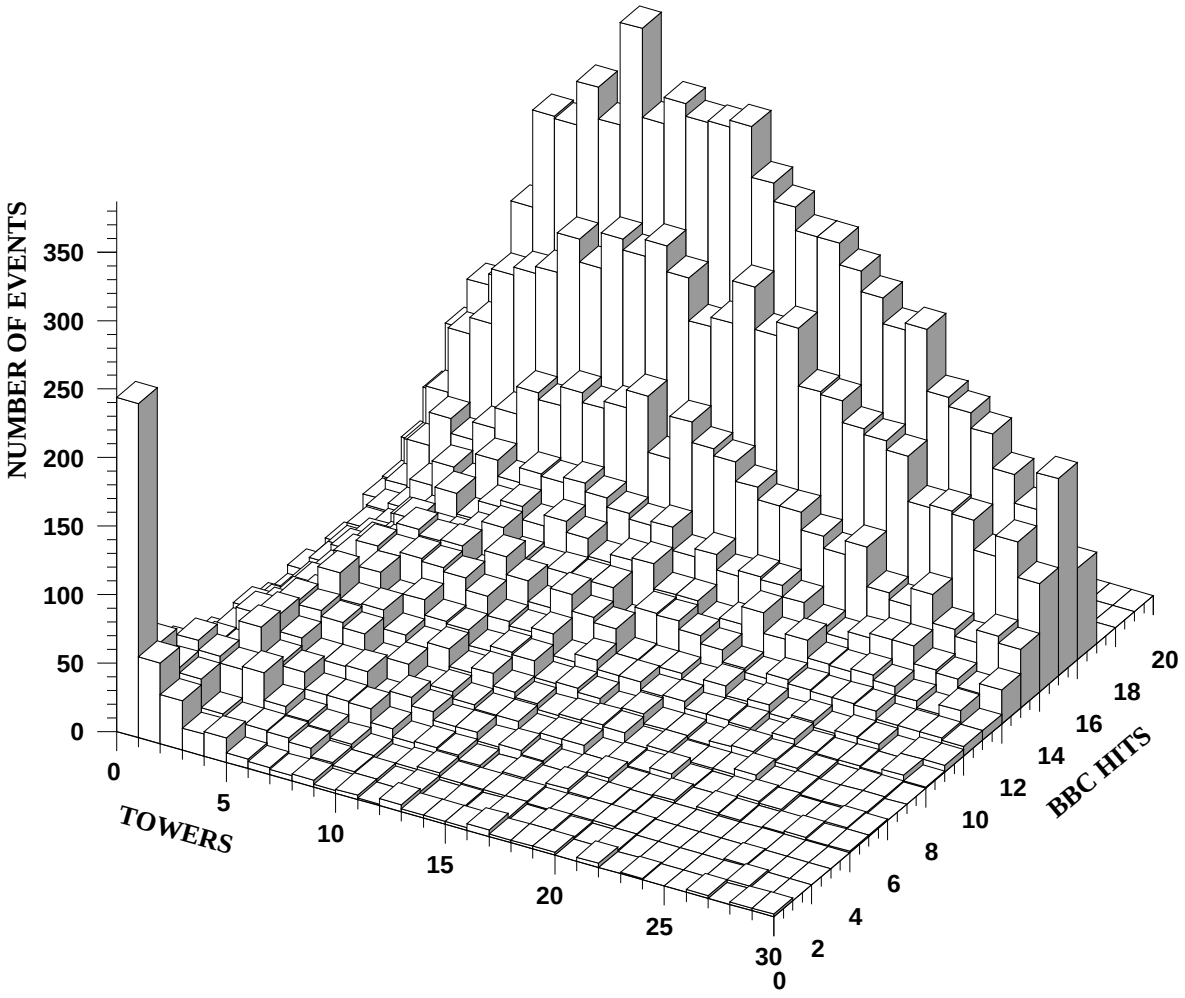

FIG. 2. Beam-beam counter multiplicity (BBC hits) versus forward calorimeter tower multiplicity in the pseudorapidity regions $3.2 < |\eta_{(BBC)}| < 5.9$ and $2.4 < |\eta_{(TOWER)}| < 4.2$ opposite the dijet system.

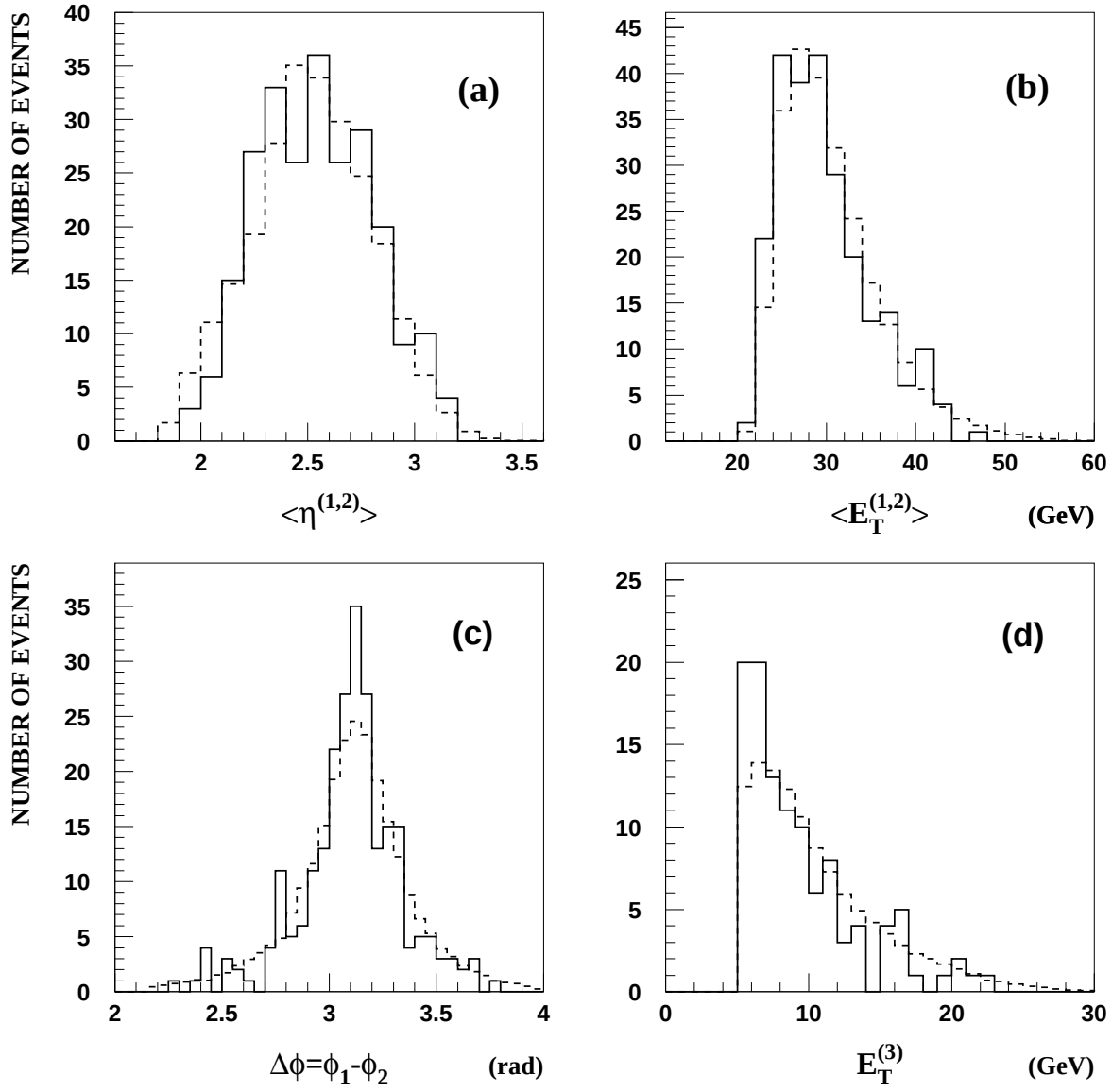

FIG. 3. Comparison of diffractive (solid) with normalized non-diffractive (dashed) event distributions: (a) average pseudorapidity, (b) average transverse energy and (c) azimuthal angle difference of the two leading jets, and (d) transverse energy of the third jet. The diffractive event sample is from the 0-0 bin of Fig. 2, which contains approximately 20% non-diffractive background.

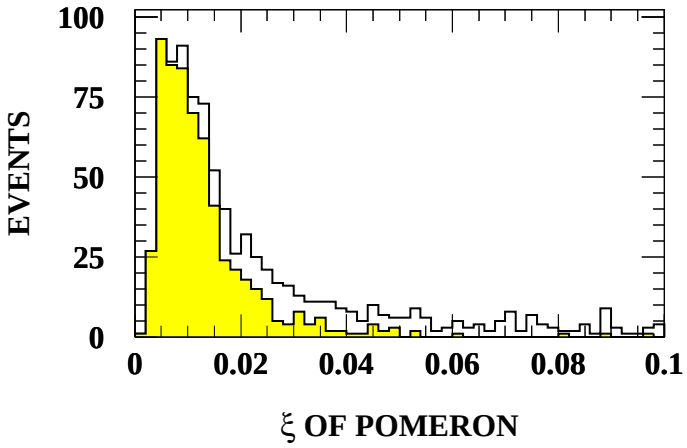

FIG. 4. Pomeron ξ distribution for diffractive dijet events with jet $E_T > 20$ GeV and $1.8 < |\eta| < 3.5$ generated by POMPYT using a hard-gluon pomeron structure. The shaded area represents the subset of Monte Carlo events with zero BBC and forward calorimeter multiplicities, corresponding to the data in the (0,0) bin of Fig. 2.

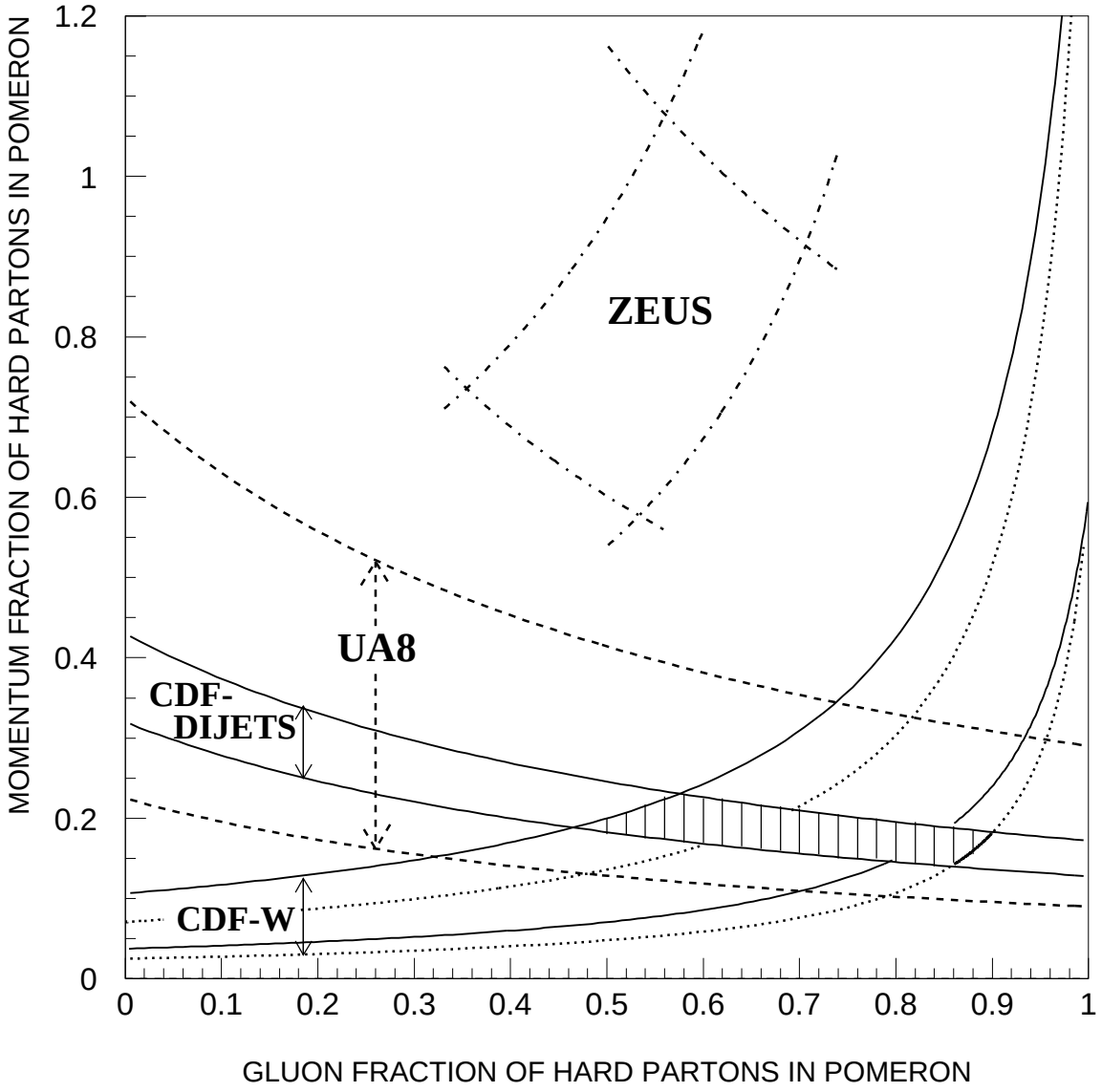

FIG. 5. Momentum fraction versus gluon fraction of hard partons in the pomeron evaluated by comparing measured diffractive rates with Monte Carlo predictions based on the standard pomeron flux and assuming that only hard pomeron partons participate in the diffractive processes considered. Results are shown for ZEUS (dashed-dotted), UA8 (dashed) and the CDF-DIJET and CDF-W measurements. The CDF W result is shown for two (dotted) or three (solid) light quark flavors in the pomeron . The shaded region is used in the text to extract the quark to gluon fraction of the pomeron and the standard flux discrepancy factor.